Two- and three-dimensional magnetic order in the layered cobalt oxychloride Sr_2CoO_3Cl

Christopher S. Knee,[1,*] Daniel J. Price,[1] Martin R. Lees,[2] and Mark T. Weller[1]
[1]*Department of Chemistry, University of Southampton, Southampton SO17 1BJ, United Kingdom*
[2]*Department of Physics, University of Warwick, Coventry CV4 7AL, United Kingdom*

(Received 18 June 2003; revised manuscript received 19 August 2003; published 7 November 2003)

The temperature dependence of the nuclear and magnetic structure of the cobalt oxychloride Sr_2CoO_3Cl has been studied using neutron powder diffraction. The material crystallizes with a structure related to K_2NiF_4 and contains two-dimensional (2D) layers of CoO_5 square pyramids that are segregated along z by alternate rocksalt SrCl and SrO blocks. The development of magnetic Bragg scattering indicates that the compound orders antiferromagnetically with a $T_N = 330(5)$ K. The phase adopts a collinear magnetic structure related to the nuclear cell by the propagation vector $\mathbf{k} = (\frac{1}{2}, \frac{1}{2}, 0)$ with the cobalt spins aligned along the a axis of the magnetic cell. The ordered moment $\mu = 2.82(3)\mu_B$, refined at 3 K, is consistent with a high-spin $(t_{2g}^4 e_g^2)$ electron configuration for the Co(III) ions. The onset of long-range magnetic order is characterized by a three-dimensional transition and is accompanied by anomalous behavior in the Co environment with distinct magnetostriction effects observed in the interlayer Co to Co exchange pathways. The transition is preceded by diffuse magnetic scattering arising from short-range in-plane correlations, with significant diffuse intensity observed up to the maximum temperature studied of 378 K. Magnetic susceptibility measurements indicate that the onset of significant 2D interactions occurs at $T \approx 500$ K. The diffuse intensity can be fitted using the Warren function to give a maximum in the 2D correlation length ξ of 40(4) Å just above T_N. Below T_N diffuse scattering coexists with magnetic Bragg scattering, indicating that the transition to long-range order is hindered most probably due to the presence of stacking disorder between the antiferromagnetic sheets.

DOI: 10.1103/PhysRevB.68.174407 PACS number(s): 75.25.+z, 61.12.Ld, 75.40.−s, 75.50.Ee

I. INTRODUCTION

The continued investigation of correlated electronic behavior exhibited by $3d$ transition-metal oxides with extended structures has also led to the development of mixed anion materials in which the oxide ion is partially replaced.[1–3] One such class of compounds is the oxide-halide family. These materials are of particular relevance to studies into cooperative behavior as they offer the potential to both control the transition-metal oxidation state, through variation of the oxide to halide ratio, and influence interlayer and intralayer separations within a particular structure type through variation in halide size. The flexibility afforded by oxyhalides is best exemplified by the wide range of oxide halide superconductors[4] developed from the K_2NiF_4 oxychloride $Sr_2CuO_2Cl_2$.[5] Following the discovery of high-T_c materials, $Sr_2CuO_2Cl_2$ and other lamellar oxyhalide cuprates have been investigated in great detail to probe the behavior of undoped superconductors,[6,7] and $Sr_2CuO_2Cl_2$ is now viewed as an ideal square lattice Heisenberg antiferromagnet.[8]

Recently cobalt oxyhalide chemistry has been extended with the report of cobalt (II) $Sr_2CoO_2X_2$ (X=Cl and Br) phases,[9] that are isostructural to $Sr_2CuO_2Cl_2$, and isolation of single crystals of the cobalt (III) Ruddlesden-Popper oxychlorides Sr_2CoO_3Cl and $Sr_3Co_2O_5Cl$ by McGlothlin *et al.*[10] In a later study the crystal structures of Sr_2CoO_3Cl and $Sr_3Co_2O_5Cl_2$ were further characterized using neutron powder diffraction at room temperature (RT).[11] The interest in cobalt oxides and oxyhalides stems from the metal's ability to adopt a number of electron configurations for a range of oxidation states in the solid state. This relationship between valence and spin state leads to a number of cobalt phases, such as $LaCoO_3$ (Ref. 12) and $TlSr_2CoO_5$ (Ref. 13), displaying unusual magnetic and electronic properties.

The present study describes the results of a variable-temperature neutron powder diffraction investigation of Sr_2CoO_3Cl which has revealed the presence of antiferromagnetic order within the material. The evolution of the cobalt spin correlation has been monitored through the growth of magnetic Bragg and diffuse scattering in the temperature range $2 \leqslant T \leqslant 378$ K. The diffraction results are interpreted alongside susceptibility measurements and provide insight into the interplay between short-range two-dimensional (2D) and long-range three-dimensional (3D) order within the material.

II. EXPERIMENT

The synthesis of polycrystalline Sr_2CoO_3Cl reported by Lourerio *et al.*[11] was achieved through reaction of SrO_2, $SrCl_2$, and Co_3O_4 and is reliant on oxidation of cobalt through the presence of excess oxygen from the decomposition of SrO_2 during phase formation to give stoichiometric Sr_2CoO_3Cl. This approach yielded a phase of reasonable purity; however, appreciable quantities of $Sr_6Co_5O_{15}$ (Ref. 14) (7.5 wt %) and $Sr_8Co_6O_{15}Cl_4$ (Ref. 15) (5.6 wt %) were also present along with an unidentified impurity phase. In an effort to improve phase purity we first synthesised the Co^{3+} precursor $Sr_2Co_2O_5$ by reaction of $SrCO_3$ and Co_3O_4 at 1000 °C (Ref. 16) and then reacted $Sr_2Co_2O_5$ with high-purity $SrCO_3$ and $SrCl_2$ in the molar ratios 1:1:1 at 850 °C for a period of 24 h. The heating was interrupted once to regrind the sample. The sample obtained was a black highly crystalline material. Long-scan powder x-ray diffraction data

 ©2003 The American Physical Society

in the 2θ range $10°-100°$ were collected on a Bruker D8 Advance diffractometer operating with Cu $K\alpha_1$ radiation and a SOLEX detector to filter the fluorescence associated with Co-containing materials. The only impurities detected were Sr_4OCl_6 (Ref. 17) and $Sr_6Co_5O_{15}$ (Ref. 14) estimated at a level of $\sim 2\%-3\%$ from the ratio of most intense Sr_2CoO_3Cl and impurity reflections.

Constant-wavelength neutron powder diffraction (NPD) were collected on a 5-g sample at 3 K on the high-resolution diffractometer D2B at the Institut Laue Langevin (ILL), France, for a period of 6 h. The sample was placed inside a 10-mm vanadium container and cooled using a Displex refrigerator. The optimum wavelength of the instrument ($\lambda = 1.5943$ Å) was utilized to obtain high-quality crystallographic data. Further scans in the temperature range 2–378 K were then obtained using the high-flux diffractometer D20 to monitor the evolving crystal and magnetic structure. The machine was operating in high-resolution mode with Soller collimators set at $10'$, a vertical 10-mm-wide monochromator window, and $\lambda = 2.4178$ Å. Scans below RT (298 K) were performed in a standard ILL cryostat and data at 298 K and above collected using a dedicated furnace. Approximate scan times of 30 min were utilized for each temperature. Analyses of the crystal and magnetic structure were then performed using the GSAS package.[18]

Magnetic susceptibility data were collected on a powder sample of Sr_2CoO_3Cl. Data in the temperature range 1.8–400 K were collected on warming using a Quantum Design MPMS-5S superconducting quantum interference device (SQUID) magnetometer in an applied field of 1 kOe. Further data were then collected using an Oxford Instruments VSM on heating from 360 K to 850 K with the sample mounted inside a furnace insert and in the same applied field.

III. RESULTS

A. Crystal and magnetic structures

The nuclear structure of Sr_2CoO_3Cl was initially determined from Rietveld analysis of the higher-resolution D2B data collected at 3 K using the atomic coordinates reported by Loureiro *et al.* as the starting model.[11] The analysis proceeded with refinement of global parameters such as background and lattice constants to give a reasonable fit to the data; however, discrepancies in the calculated intensity were apparent for certain reflections. This effect was attributed to a preferred orientation arising from the platelike morphology of the crystallites within the sample and was corrected satisfactorily using the March-Dollase function.[19] The positional and atomic displacement parameters for the individual atoms were then varied. In the closing stages of the refinement the occupancy of each site was permitted to vary and no significant site deficiencies were detected, indicating that the minor impurity levels of $Sr_6Co_5O_{15}$ (2.6 wt %) and Sr_4OCl_6 (1.5 wt %) have no effect on the stoichiometry of the main phase. Table I summarizes the structural parameters derived from the refinement and the fit achieved to the data is shown in Fig. 1. Analysis of the lower-resolution D20 data employed the atomic coordinates determined from the D2B analysis in initial cycles and followed the same refinement procedure.

TABLE I. Refined structural parameters for Sr_2CoO_3Cl at 3 K determined from analysis of D2B data. Space group $P4/nmm$. Weight percent Sr_2CoO_3Cl (95.9%), $Sr_6Co_5O_{15}$ (2.6%), and Sr_4OCl_6 (1.5%). Fit factors $R_{wp}=4.83\%$, $R_p=3.51\%$, $\chi^2=5.43$. Preferred orientation coefficient $R_o=1.20(2)$.

Atom	Site	z	$U_{iso}\times 100$ (Å^2)	n
Sr(1)	$2c$ $(\frac{1}{4},\frac{1}{4},z)$	0.098(1)	0.08(4)	1.0
Sr(2)	$2c$ $(\frac{1}{4},\frac{1}{4},z)$	0.3452(1)	0.55(5)	1.0
Co	$2c$ $(\frac{1}{4},\frac{3}{4},z)$	0.2049(4)	0.21(9)	1.0
O(1)	$4f$ $(\frac{3}{4},\frac{1}{4},z)$	0.2294(1)	0.48(3)	1.0
O(2)	$2c$ $(\frac{3}{4},\frac{3}{4},z)$	0.0747(2)	0.41(4)	1.0
Cl	$2c$ $(\frac{3}{4},\frac{3}{4},z)$	0.4252(1)	0.65(3)	1.0
a			3.88716(3) Å	
c			14.2775(2) Å	
Magnetic cell			$a_M=b_M=\sqrt{2}a,\ c_M=c$	
μ			$2.82(3)\mu_B$	

Additional Bragg reflections were observed in the NPD scans that could not be accounted for by the nuclear model of Sr_2CoO_3Cl. The low-angle position of the peaks indicated that they might be magnetic in origin and this was confirmed by variable-temperature scans performed on D20, which showed that the reflections vanished above $T=338$ K (Fig. 2). The reversibility of the magnetic transition was then established on cooling back to RT. The magnetic intensities could be indexed on the basis of an orthorhombic magnetic cell related to the nuclear cell by $a_{mag}=b_{mag}=\sqrt{2}a_{nuc}$ and $c_{mag}=c_{nuc}$. For a collinear magnetic structure this implies a propagation vector $\mathbf{k}=(\frac{1}{2},\ \frac{1}{2},\ 0)$. The most intense magnetic peaks were identified as the (101), (102), and (103) reflections analogous to the behavior observed for the K_2NiF_4

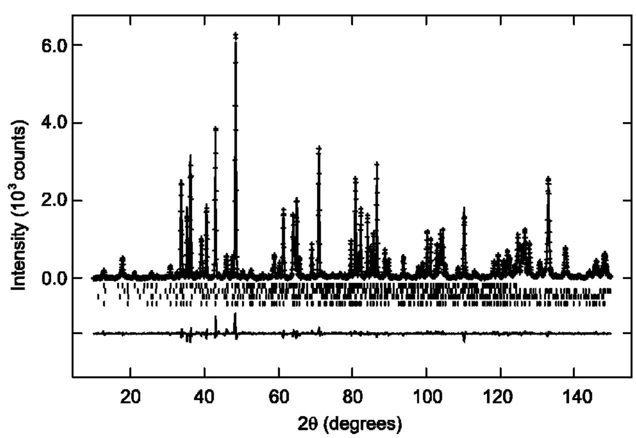

FIG. 1. The NPD pattern obtained for Sr_2CoO_3Cl on D2B ($\lambda = 1.5943$ Å) at 3 K. Crosses are observed data; lines are calculated and difference plots. Vertical tick marks indicate the position of allowed reflections for the nuclear structure of Sr_2CoO_3Cl (bottom) and magnetic structure (top). Reflections for the minor impurities Sr_4OCl_6 (lower middle) and $Sr_6Co_5O_{15}$ (upper middle) are also shown.

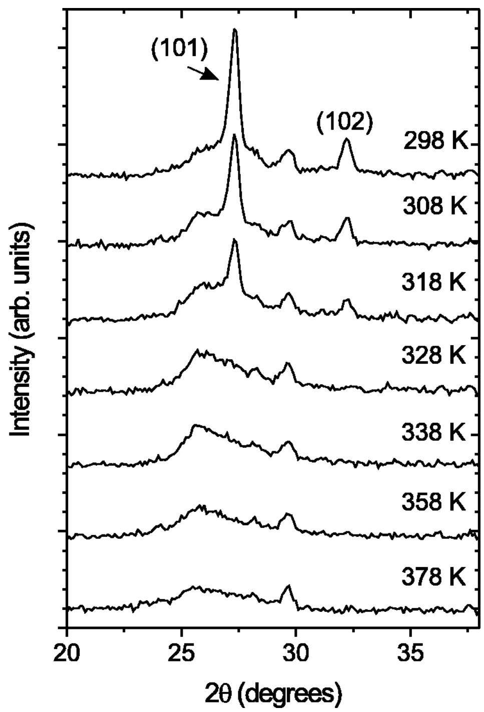

FIG. 2. The temperature dependence of the magnetic scattering exhibited by Sr_2CoO_3Cl in the T range 298–378 K. The positions of the two most intense magnetic Bragg reflections are labeled.

phases La_2NiO_4 (Ref. 20) and $PrCaCrO_4$ (Ref. 21). The magnetic form factor of Co^{3+} was used[22] and an excellent fit to the data (Fig. 3) achieved with the cobalt spins aligned along the x direction to form antiferromagnetic layers within the ab plane and nearest moments in neighboring layers stacked to form antiferromagnetic sheets in the ac plane. Alternatively the spin direction could be chosen to lie along the y directionwith A-type centering to yield an equivalent result. Models with a component of the moment along z were tested; however, this led to a deterioration of the fit and any experimentally significant canting of the spins out of the basal plane can be discounted. The temperature dependence of the (101) and (102) magnetic reflections allows the $T_{\text{Néel}}$ to be estimated as 330(5) K.

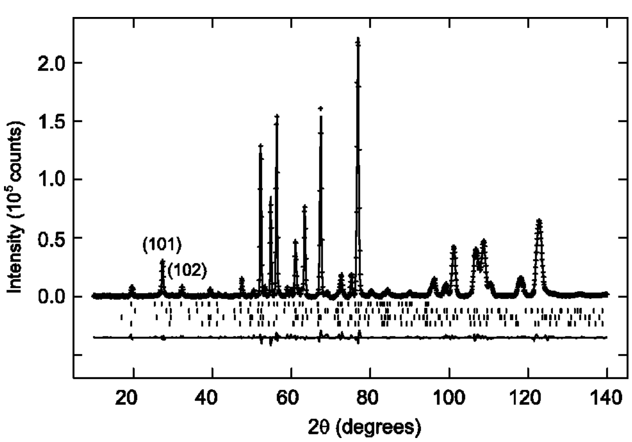

FIG. 3. The NPD pattern obtained for Sr_2CoO_3Cl on D20 at 2 K. The plot follows the same labeling style as in Fig. 1. Also indicated are the (101) and (102) magnetic reflections of Sr_2CoO_3Cl.

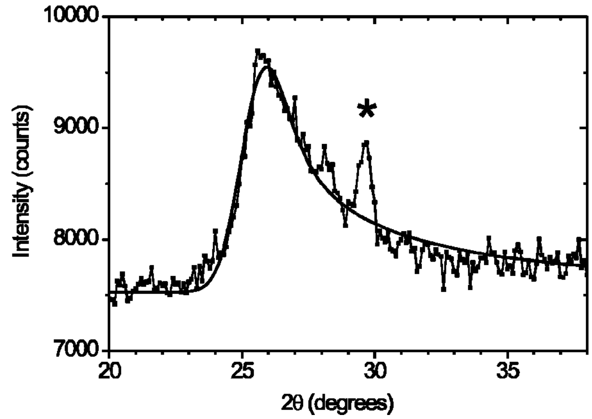

FIG. 4. Fit of diffuse scattering achieved using the Warren function to D20 data collected at $T=338$ K ($\lambda=2.4178$ Å). The marked Bragg reflection corresponds to an impurity which was excluded from the fitting process.

B. Two-dimensional correlation length

In addition to the coherent Bragg scattering a broad asymmetric feature centered at $2\theta\sim25.5°$ (d spacing ≈5.5 Å) was also apparent. The shape of this feature, which is evident even at the highest experimental temperature of 378 K, is seen to sharpen on cooling until the T_N is reached. Cooling below T_N sees the growth of magnetic Bragg peaks at the expense of the asymmetric diffuse peak (Fig. 2). Remarkably there is a wide temperature range below T_N where both coherent magnetic Bragg scattering and diffuse scattering coexist. Even at 200 K there appears to be a weak diffuse peak underneath the strong (101) magnetic reflection. This diffuse magnetic scattering arises from short-range 2D spin-spin correlations and its position corresponds to the (10) reflection of a short-range-ordered system. The intensity was fitted using the Warren function[23] [Eq. (1)] to obtain an estimate of the 2D spin-spin correlation length ξ for temperatures at and above 298 K. The scattered power is given by

$$P(\theta)=KmF_{hk}^2\frac{(1+\cos^2 2\theta)}{2(\sin\theta)^{3/2}}\left(\frac{\xi}{\lambda\sqrt{\pi}}\right)^{1/2}F(a), \qquad (1)$$

where

$$a=\frac{2\xi\sqrt{\pi}}{\lambda}(\sin\theta-\sin\theta_0) \qquad (2)$$

and K is a scale factor, λ is the neutron wavelength, and m is the multiplicity of the 2D reflection (hk) centered at θ_0 with structure factor F_{hk}. The function $F(a)$ was evaluated numerically as described previously.[24]

All diffraction patterns collected at and above 298 K were fitted between $20°<2\theta<38°$ with data in the vicinity of the impurity nuclear reflection at 29.6° being excluded. For measurements performed at 318 K and below it was necessary to also exclude data in the vicinity of the (101) and (102) magnetic Bragg peaks. In the absence of a full spin polarization analysis the diffuse magnetic scattering was estimated to be at most only $\sim25\%$ of the background at the peak maximum and qualitatively good fits (Fig. 4) to the Warren function

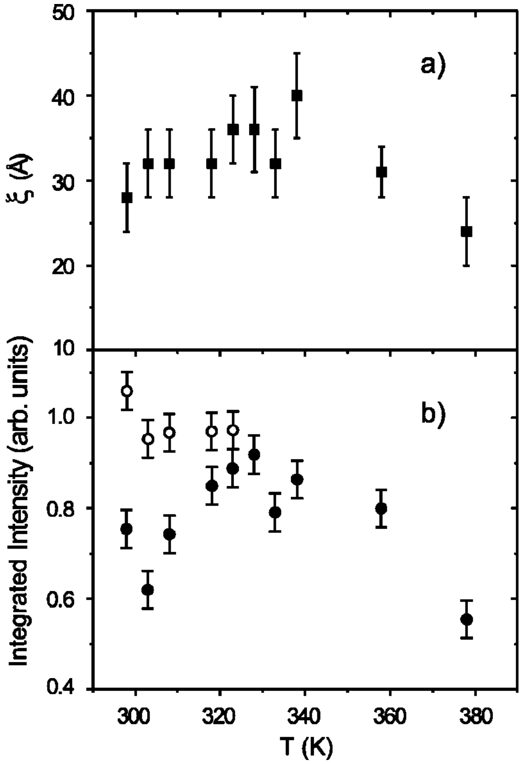

FIG. 5. The two-dimensional magnetic correlation length ξ of Sr_2CoO_3Cl as a function of temperature (a). (b) shows the thermal evolution of the diffuse scattering intensity (filled circles) and the total integrated magnetic intensity (open circles) which includes the Warren peak and the magnetic Bragg reflections in the range $20° \leqslant 2\theta \leqslant 38°$. The data were normalized with respect to the (002) nuclear peak at 19.6°.

were achieved by subtracting a simple linear background function. The thermal dependence of the correlation length ξ through the long-range-ordering transition is shown in Fig. 5(a). Also shown in Fig. 5(b) are the temperature dependence of the diffuse intensity and the behavior of the total magnetic scattering in the same 2θ region.

C. Magnetic susceptibility

The temperature dependence of the magnetic susceptibility of Sr_2CoO_3Cl in the temperature range 10–850 K is plotted in Fig. 6. The molar susceptibility passes through a broad maxima centered at $T \approx 500$ K (see inset) and then drops slowly on cooling, reaching a minimum at ≈ 200 K. At very low temperatures χ shows a rise attributed to the $Sr_6Co_5O_{15}$ impurity.[25] The increase in scatter observed for the high-temperature data reflects the decreased sensitivity and greater level of background signal associated with the vibrating-sample-magnetometer (VSM) measurement. Imperfect background subtraction for the VSM data accounts for the small discrepancy in the measured susceptibility between the two data sets.

IV. DISCUSSION

The presence of magnetic Bragg scattering in all neutron powder data sets collected below 328 K for Sr_2CoO_3Cl reveals the presence of antiferromagnetic long-range order (AFLRO) of the cobalt spins in the material. The original room-temperature neutron diffraction study by Loureiro *et al.*[11] did not report this behavior and concluded from susceptibility measurements that no magnetic order was present in the compound. Initially, differences in the synthetic method and phase purity of the respective samples seemed to be the most likely reason for this contrasting behavior. For example any small oxygen deficiency within the material could significantly affect the chances of observing magnetic order, particularly the long-range correlation required for coherent Bragg scattering. However, from inspection of the low-angle neutron data presented in Ref. 11 we now conclude that the three additional peaks observed in the region 16°–30° were wrongly identified as an impurity and were in fact of magnetic origin. Possibly the poorer phase purity and the absence of variable-temperature scans contributed to the magnetic scattering being overlooked.

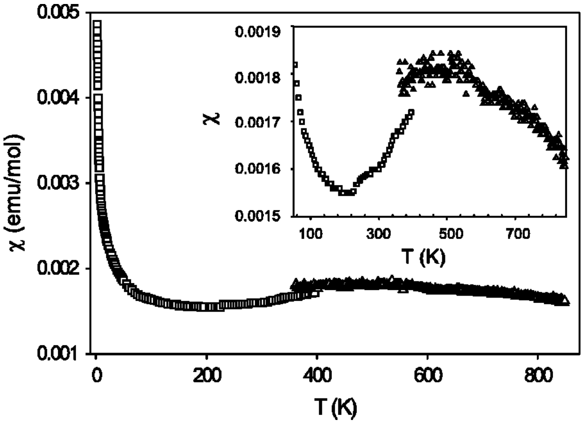

FIG. 6. The temperature dependence of the magnetic susceptibility of Sr_2CoO_3Cl on warming in an applied field of 1 kOe. Open squares and open triangles are data collected using the SQUID and VSM magnetometers, respectively. The inset shows an expanded area for the temperature range 60–820 K.

The crystal and magnetic structures of Sr_2CoO_3Cl are shown in Fig. 7 in which the close structural analogy between the phase and the K_2NiF_4 structure is apparent. The large chloride ion effectively replaces one of the terminal apical oxygen positions of the perovskite block of the K_2NiF_4 phase $LaSrCoO_4$ (Ref. 26). Ordering of the chloride ion along z, rather than random replacement of oxide, leads to a reduction of the cell symmetry from the $I4/mmm$ of ideal K_2NiF_4 phases to $P4/nmm$. Significantly the presence of the chloride ion results in alternate CoO_2 layer separations of 5.85 Å and 8.42 Å along the c direction rather than the regular $c/2$ stacking of K_2NiF_4. A further structural subtlety is that the cobalt ions are shifted along z away from the basal plane of the CoO_5 square pyramids and this gives rise to a high level of buckling—i.e., a O(1)-Co-O(1) bond angle $\approx 162°$ compared with the flat 180° planes observed in standard 0201 phases.

The cobalt spins within Sr_2CoO_3Cl are aligned in an antiparallel manner in the ab plane of the magnetic cell. This arrangement leads to two possibilities for the relative orientation of the nearest-neighbor layers as illustrated by the re-

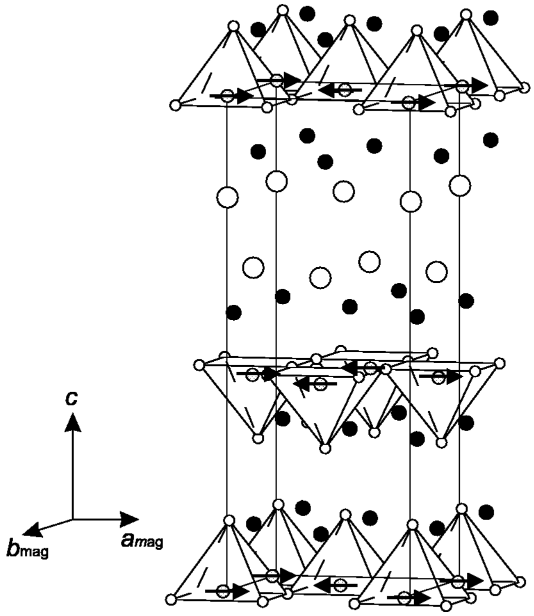

FIG. 7. Nuclear and magnetic structure of Sr_2CoO_3Cl. Large open spheres represent chloride ions, medium shaded spheres cobalt, small open spheres oxygen, and black medium spheres are strontium sites. The cobalt coordination is depicted as square pyramidal with respect to oxygen. The cobalt spin direction and magnetic cell are shown.

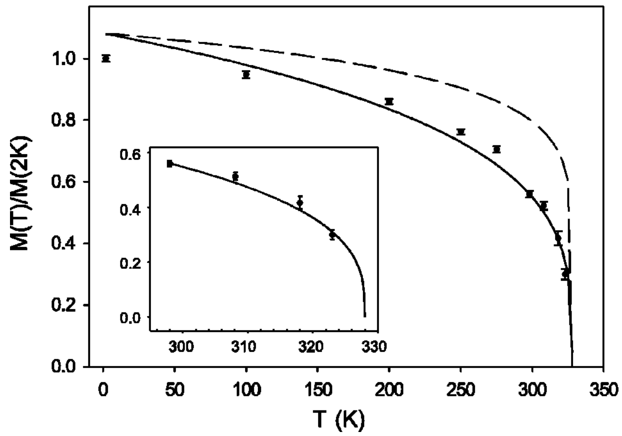

FIG. 8. Sublattice magnetization as a function of temperature for Sr_2CoO_3Cl. The data are fitted using the power law of Eq. (3) (solid line) and also shown is the expected behavior for the 2D Ising model (dashed line). The inset shows the fit to the power law in the critical region.

lated K_2NiF_4 phases La_2NiO_4 (Ref. 20) and La_2CuO_4 (Ref. 27). The absence of the (100) reflection for Sr_2CoO_3Cl enables the spin arrangement shown in Fig. 7 to be identified in which an antiferromagnetic (AF) relationship between neighboring spins located in the ac plane is favored. In comparison a ferromagnetic arrangement is observed for both La_2CuO_4 and $Sr_2CuO_2Cl_2$ (Ref. 6). It is noteworthy that for 2D antiferromagnets such as K_2NiF_4 itself[28] and the manganese oxychloride Sr_2MnO_3Cl (Ref. 29), with spin directions confined to the tetragonal axis this subtlety does not arise. In their paper on the magnetism of $Sr_2CuO_2Cl_2$ Vaknin *et al.*[6] have shown that for purely dipolar interactions the magnetic structure observed for La_2CuO_4 is favored rather than the spin arrangement adopted by La_2NiO_4 and now observed for the cobalt oxychloride. Therefore it seems likely that interlayer exchange coupling, rather than through-space dipolar interactions, governs both the spin structure and the transition to LRO within Sr_2CoO_3Cl.

The refined moment of $2.82(3)\mu_B$ obtained at 3 K from the D2B data is in agreement with the presence of high-spin Co^{3+} ($S=2$) once the expected reductions commonly observed for the static moment in related 2D systems due to zero-point fluctuations and covalency effects are taken into account. The magnitude of the moment, however, does not preclude the presence of a level of the intermediate, $S=1$, spin state that is known to occur in distorted chemical environments.[13] Furthermore, determination of the spin state may be complicated by partially quenched orbital interactions for the cobalt ion, a conclusion that is supported by the $\mu_{eff}=6.8\mu_B$ obtained from the high-temperature susceptibility data (600–850 K), and further studies are required for a definitive assignment of the cobalt electronic configuration.

The temperature dependence of the normalized moment in the temperature range 2–340 K along with a fit to the power law given in Eq. (3) below is shown in Fig. 8. Also shown is the expected behavior for a 2D Ising model (i.e., critical exponent $\beta=0.125$):

$$\frac{M(T)}{M(0)}=C(1-T/T_N)^{\beta}. \tag{3}$$

A reasonable fit over the whole temperature rage was obtained with $C=1.08(4)$, $T_N=328(4)$ K, and $\beta=0.28(3)$. If the fit is instead limited to the critical region (see inset), then excellent agreement is obtained with $C=1.2(2)$, $T_N=328(1)$ K, and $\beta=0.33(5)$ consistent with a 3D transition. This behavior contrasts with that exhibited by classical 2D systems such as K_2NiF_4 (Ref. 28) and K_2FeF_4 (Ref. 30) which display 2D Ising-type transitions with $\beta\sim0.15$. The transition from 2D correlations to long-range order in K_2NiF_4 occurs within a 1 K window either side of T_N as LRO is established essentially in two dimensions and 3D order follows parasitically. In contrast the behavior of Sr_2CoO_3Cl is characterized by a more gradual transition that is consistent with interlayer coupling playing a significant part in the growth of LRO in the material. In this respect Sr_2CoO_3Cl is similar to La_2CuO_4 (Ref. 31).

The appearance of coherent magnetic Bragg scattering is preceded by diffuse scattering arising from short-range 2D correlations confined to the basal CoO_2 planes. The sharpening of the Warren peak on cooling from 378 to 338 K (Fig. 2) is clearly associated with a steady increase in the 2D correlation length which reaches a maximum of 40 Å at 338 K just above T_N (Fig. 5). In theory for such a second-order phase transition we expect a divergence of ξ to infinity at T_N, followed by a crossover to long-range 3D ordering, whereupon the Warren feature should disappear as magnetic Bragg peaks are formed. We do not observe such an abrupt transition. Instead both diffuse scattering and magnetic Bragg peaks coexist over a large thermal region. This behavior indicates that the transition to 3D LRO is hindered in some areas of the sample and the most likely explanation for this lies with the microstructure of the sample used in the current study. For example the presence of stacking faults along *c* will severely affect the 3D correlation within the material. Physically the occurrence of stacking disorder within Sr_2CoO_3Cl is likely given the presence of an easy plane of cleavage along the relatively weakly bonded double SrCl layers. The significant preferred orientation observed for the diffraction patterns of the finely ground sample provides strong evidence that such a cleavage plane is present in the material. In addition it is possible that occasional intergrowths of the closely related double- and triple-layer phases $Sr_3Co_2O_5Cl_2$ (Ref. 10) and $Sr_8Co_6O_{15}Cl_4$ (Ref. 15) occur. These would also significantly disrupt the interlayer coherence required for 3D Bragg intensity.

The maximum in correlation length, $\xi = 40(4)$ Å, corresponds to a coherence length that extends within the *xy* plane for ca. 10 unit cells before diminishing to approximately half that value at 378 K (Fig. 5). In comparison a value of >200 Å has been determined for La_2CuO_4 above T_N (Ref. 31) and a recent study of the K_2NiF_4 manganite family $Ba_xSr_{1-x}LaMnO_4$ $(0<x<0.30)$ reported a $\xi = 21(3)$ Å for the $x=0.06$ member.[32] The values obtained below T_N remain static at around 30 Å and this may provide an estimate of the size of the two-dimensionally correlated domains that persist below T_N due to static disorder.

The temperature dependence of the magnetic susceptibility of Sr_2CoO_3Cl (Fig. 6) provides further evidence of the 2D magnetic character of the material at temperatures above T_N. The broad transition observed between 400 and 600 K is a signature of short-range AF correlations in a planar system and indicates the onset of significant 2D order at $T_{\chi\,\max} \sim 500$ K. Between 500 K and 330 K the strength of these in-plane correlations grows until ξ reaches a critical point at T_N as defined by Eq. (4) and 3D ordering becomes energetically favorable:[33]

$$T_N \approx \left(\frac{\xi}{a}\right)^2 J_z S^2 / k_B. \tag{4}$$

Taking $\xi = 40$ Å, the cell parameter $a = 3.9$ Å, and $S=2$ allows the value of the interlayer exchange $J_z = 0.78$ K to be estimated. The strength of the intraplanar J_{xy} interaction can also be evaluated using Line's formula[34] and taking $T_{\chi\,\max} = 500$ K yields a $J_{xy} = 74.3$ K:

$$\frac{k_B T_{\chi\,\max}}{J_{xy}} = 1.12 S(S+1) + 0.10, \tag{5}$$

indicating that the J_z interaction within Sr_2CoO_3Cl is approximately two orders of magnitude weaker than the in-plane superexchange coupling.

Having characterized the thermal behavior of the magnetic correlations within Sr_2CoO_3Cl our attention now focuses on the phase's crystal structure. The temperature dependences of the lattice parameters and cell volume derived from analysis of the D20 data over the complete temperature range of study are shown in Fig. 9. From these data it is clear that the onset of LRO at the $T_N \sim 330$ K is not accompanied by a gross structural transition. Strictly, the symmetry is reduced from tetragonal to orthorhombic at the magnetic phase transition. This lowering of symmetry is expected to relieve the degeneracy associated with the interlayer exchange pathways of the tetragonal cell and stabilize the observed spin structure. Indeed the related double-layer Ruddlesden-Popper phase $Sr_2Y_{0.8}Ca_{0.2}Co_2O_6$ (Ref. 35) has recently been shown to undergo a large orthorhombic distortion at the onset of LRO, emphasizing the link between spin and structural degrees of freedom. However, no detectable peak splitting was observed in the D20 data on crossing T_N. To further test for a reduction in symmetry below T_N the high-resolution D2B data collected at 3 K were analyzed using an orthorhombic cell. A stable refinement could be obtained with parameters $a = 3.88556(8)$ Å and $b = 3.88875(8)$ Å, and a small improvement in the agreement statistics, $\chi^2 = 5.25$, $R_{wp} = 4.74\%$, and $R_p = 3.44\%$ compared with 5.43, 4.83%, and 3.51%, respectively, in $P4/nmm$, was obtained. However, the refined distortion $b/a \sim 1.0005$ lies on the limit of the resolution of D2B and the enhancement in the least-squares fit may merely reflect the additional complexity of the structural model. Therefore from our diffraction data the average nuclear structure of Sr_2CoO_3Cl is best described as tetragonal throughout the measured temperature range.

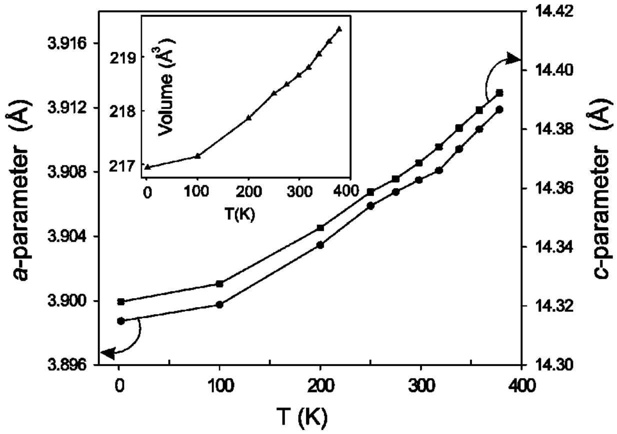

FIG. 9. The temperature dependence of the lattice constants (*a* and *c*) of Sr_2CoO_3Cl. The inset shows the thermal behavior of the unit cell volume.

Figure 10 shows the cobalt bond distances and the in-plane Co-O(1)-Co bond angles obtained at 298 K and above. The plots provide evidence of anomalous behavior in the temperature region close to the onset of LRO. Both the Co-O(1) in-plane and Co-Cl apical separations remain constant between 380 K and 340 K before contracting on cooling below 340 K. Coincidentally the Co-O(1)-Co basal bond angle appears to undergo a weak change, flattening out and reducing the extent of buckling. The structural response can be related to the possible AF exchange pathways within Sr_2CoO_3Cl. As T_N is associated with the onset of 3D order in the material the pathways between adjacent Co ions separated along *z* by the rocksalt Sr-O and Sr-Cl layers are of particular interest. Figure 11 shows the two shortest possible exchange pathways across these layers, with a four-bond link

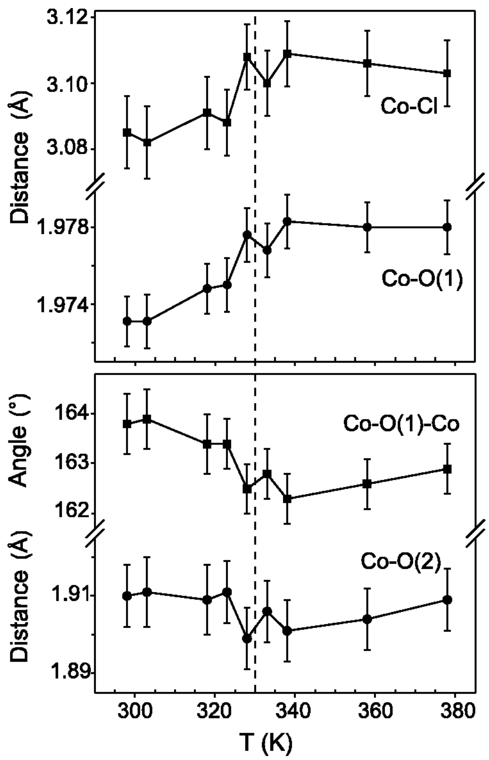

FIG. 10. The temperature dependence of the cobalt environment in Sr_2CoO_3Cl as T_N is crossed. The dashed lines coincides with $T = 330$ K.

mediated through the Sr(1)-O(2) bond and a four-bond pathway through the Cl-Sr(2) bridge. For the sake of clarity only one of the equivalent possibilities for each pathway has been highlighted. Both distances show significant changes close to the onset of LRO, with distance J_1 passing through a distinct minimum and J_2 showing a sharp decrease [Fig. 12(a)], suggesting that these interactions play a critical role in the interlayer magnetic propagation. This behavior leads to a reduction in the separation of Co ions across the rocksalt SrCl layers of approximately 0.06 Å between 338 K and 298 K [Fig. 12(b)] and represents a small magnetostriction associated with T_N. The structural response, although discernible, is weak and compatible with the magnetic transition involving a crossover from strong existing 2D interactions to longer-range 3D correlations in the material.

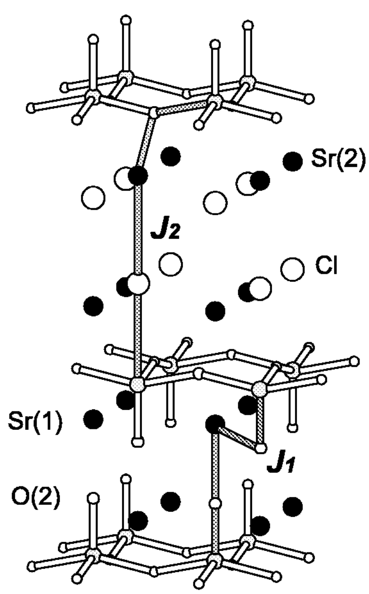

FIG. 11. Possible interlayer exchange pathways within Sr_2CoO_3Cl. J_1 is a four-bond pathway through the Sr(1)-O(2) layers and J_2 is a four-bond pathway through the Sr(2)-Cl layers.

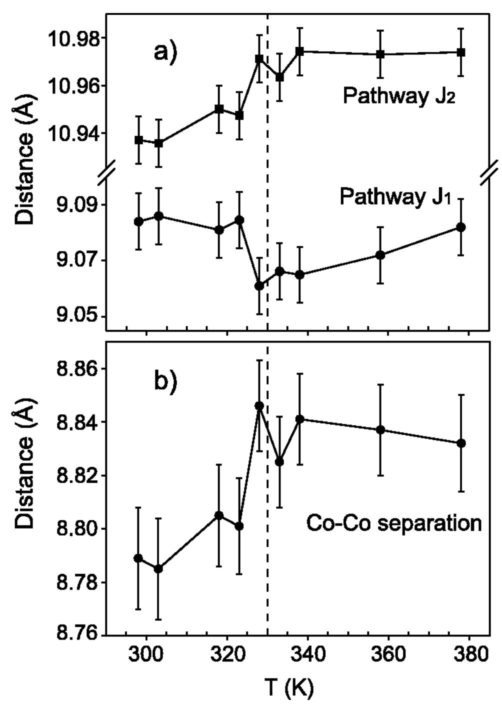

FIG. 12. Interlayer magnetic pathway distances (a) and through-space Co to Co separation across the SrCl double layers (b) in the temperature range 298–380 K.

V. CONCLUSION

The magnetism of the layered oxychloride Sr_2CoO_3Cl exhibits a transition from short-range two-dimensional correlations to long-range three-dimensional order. The crossover occurs at $T_N = 330(5)$ K and is characterized by a 3D transition rather than the 2D Ising-like behavior that may have been expected given the material's highly anisotropic structure. In the AFLRO state the cobalt spins are confined to the tetragonal plane and align with a spin structure analogous to that previously described for La_2NiO_4. Both the spin arrangement and the nature of the transition indicate that exchange-mediated interactions are responsible for the Co ordering, an interpretation that is further supported by the weak magnetostriction observed in the interlayer exchange pathways at the onset of LRO. Two-dimensional correlations persist below T_N and it is believed that stacking disorder of the antiferromagnetic sheets restricts extended 3D correlation. In this respect further measurements on a high-quality single crystal would be beneficial to accurately gauge the effect such structural disorder has on the magnetic correlation within Sr_2CoO_3Cl.

ACKNOWLEDGMENTS

The authors are grateful to the EPSRC for Grant Nos. GR/R99591/01 and GR/M21836/01 in aid of this work. D.J.P. wishes to acknowledge the EPSRC for support. We also thank the Institut Laue Langevin for the provision of neutron diffraction facilities and Alan Hewat and Thomas Hansen for their technical assistance while performing the experiments.

*Corresponding author. Electronic address: csk@soton.ac.uk

[1] K. Yamaura, Q. Huang, J.W. Lynn, R.W. Erwin, and R.J. Cava, J. Solid State Chem. **152**, 374 (2000).
[2] G.M. Veith, M. Greenblatt, M. Croft, and J.B. Goodenough, Mater. Res. Bull. **36**, 1521 (2001).
[3] K. Otzschi, H. Ogino, J. Shimoyama, and K. Kishio K, J. Low Temp. Phys. **117**, 729 (1999).
[4] S. Adachi, T. Tatsuki, T. Tamura, and K. Tanabe, Chem. Mater. **10**, 2860 (1998).
[5] B. Grande and Hk. Müller-Buschbaum, Z. Anorg. Allg. Chem. **417**, 68 (1975).
[6] D. Vaknin, S.K. Sinha, C. Stassis, L.L. Miller, and D.C. Johnston, Phys. Rev. B **41**, 1926 (1990).
[7] F.C. Chou, A. Aharony, R.J. Birgeneau, O. Entin-Wohlman, M. Greven, A.B. Harris, M.A. Kastner, Y.J. Kim, D.S. Kleinberg, Y.S. Lee, and Q. Zhu, Phys. Rev. Lett. **78**, 535 (1997).
[8] M. Greven, R.J. Birgeneau, Y. Endoh, M.A. Kastner, M. Matsuda, and G. Shirane, Z. Phys. B: Condens. Matter **96**, 465 (1995).
[9] C.S. Knee and M.T. Weller, J. Solid State Chem. **168**, 1 (2002).
[10] N. Mcglothlin, D. Ho, and R.J. Cava, Mater. Res. Bull. **35**, 1035 (2000).
[11] S.M. Loureiro, C. Felser, Q. Huang, and R.J. Cava, Chem. Mater. **12**, 3181 (2000).
[12] C. Zobel, M. Kriener, D. Bruns, J. Baier, M. Gruninger, T. Lorenz, P. Reutler, and A. Revcolevschi, Phys. Rev. B **66**, 020402 (2002).
[13] J.P. Doumerc, M. Coutanceau, A. Demourgues, E. Elkaim, J.C. Grenier, and M. Pouchard, J. Mater. Chem. **11**, 78 (2001).
[14] W.T.A. Harrison, S.L. Hegwood, and A.J. Jacobson, J. Chem. Soc., Chem. Commun. **19**, 1953 (1995).
[15] Hk. Müller-Buschbaum and J. Boje, Z. Anorg. Allg. Chem. **592**, 73 (1991).
[16] J.C. Grenier, S. Ghodbane, G. Demazeau, M. Pouchard, and P. Hagnemuller, Mater. Res. Bull. **14**, 831 (1979).
[17] O. Reckeweg and H. Meyer, Z. Kristallogr. **212**, 235 (1997).
[18] A.C. Larson and R.B. von Dreele, *General Structure Analysis System* (Los Alamos National Laboratory, Los Alamos, 1994).
[19] W.A. Dollase, J. Appl. Crystallogr. **19**, 267 (1986).
[20] G. Aeppli and D.J. Buttrey, Phys. Rev. Lett. **61**, 203 (1988).
[21] J.R. de Paz, M.T. Fernandez-Diaz, J.H. Velasco, R.S. Puche, and J.L. Martinez, Solid State Chem. **142**, 29 (1999).
[22] P.J. Brown, *International Tables for Crystallography* (Kluwer Academic, Dordrecht, 1992), Vol. C, p. 391.
[23] B.E. Warren, Phys. Rev. **59**, 693 (1941).
[24] S.G. Carling, D. Visser, D. Hautot, I.D. Watts, P. Day, J. Ensling, P. Gutlich, G.J. Long, and F. Grandjean, Phys. Rev. B **66**, 104407 (2002).
[25] G. Demazeau, P. Courbin, G. Le Flem, M. Pouchard, P. Hagenmueller, J.L. Soubeyroux, I.G. Main, and G.A. Robins, Nouv. J. Chim. **3**, 171 (1979).
[26] H. Taguchi, M. Shimada, and M. Koizumi, J. Solid State Chem. **29**, 221 (1979).
[27] D. Vaknin, S.K. Sinha, D.E. Moncton, D.C. Johnston, J.M. Newsam, C.R. Safinya, and H.E. King, Jr., Phys. Rev. Lett. **58**, 2802 (1987).
[28] R.J. Birgeneau, H.J. Guggenheim, and G. Shirane, Phys. Rev. B **1**, 2211 (1970).
[29] C.S. Knee, A.A. Zhukov, and M.T. Weller, Chem. Mater. **14**, 4249 (2002).
[30] M.P.H. Thurlings, E. Frikkee, and H.W. de Wijn, Phys. Rev. B **25**, 4750 (1982).
[31] G. Shirane, Y. Endoh, R.J. Birgeneau, M.A. Kastner, Y. Hidaka, M. Oda, M. Suzuki, and T. Murakami, Phys. Rev. Lett. **59**, 1613 (1987).
[32] M. Bieringer and J.E. Greedan, J. Mater. Chem. **12**, 279 (2002).
[33] L.J. de Longh, *Magnetic Properties of Layered Transition Metal Compounds* (Kluwer Academic, Boston, 1990), p. 19.
[34] M.E. Lines, J. Phys. Chem. Solids **31**, 101 (1970).
[35] K. Yamaura, Q. Huang, R.W. Erwin, J.W. Lynn, and R.J. Cava, Phys. Rev. B **60**, 9623 (1999).